SHEAR SPECIFIC STIFFNESS OF FRACTURES AND FRACTURE INTERSECTIONS

BRADLEY C. ABELL*, MIN-KWANG CHOI†, AND LAURA J. PYRAK-NOLTE‡

Abstract. Fractures in rock masses influence strongly the mechanical and hydraulic properties of a rock mass. Thus, the detection and characterization of fractures using geophysical methods is of critical importance for maintaining the integrity of sub-surface infrastructure and subsurface waste or storage repositories. While the effects of single fractures or sets of parallel fractures on seismic wave propagation have been studied by many scientists and engineers, little research has been performed to determine the role of fracture intersections on seismic wave attenuation and velocity. A fundamental question is whether the specific stiffness or compliance of an intersection is the same or differs from the stiffness of any of the individual fractures within two intersecting sets of fractures. In this paper, we show from experimental and numerical studies that the stiffness of fracture intersections can be less than, equal to, or greater than the stiffness of the individual fractures depending on the applied bi-axial loading conditions.

1. Introduction. Rock fractures often occur in sets, as networks, or singly on nearly all length scales. Although many fracture sets contain parallel fractures, sets with orthogonal intersecting fractures are also common. Orthogonal fractures are prevalent in many geologic formations found in Norway, the United States, the United Kingdom, and even on extraterrestrial bodies such as the Moon [1-4].

Extensive theoretical, computational and experimental research has examined the effect of single fractures and fracture sets in isotropic and anisotropic media on seismic wave propagation [5-13]. Hydraulic studies on similar fractures have also been conducted as well as for intersecting fractures [14-23]. It is surprising then, that so little work has been done on characterizing orthogonal fracture intersections seismically.

From the aforementioned studies on single and parallel sets of fractures, fractures give rise to converted modes, guided modes, and anisotropy. An example of a guided mode is a fracture interface wave, i.e. a Rayleigh wave that travels along or is guided by a single fracture.

Interface waves exist at non-welded contacts such as fractures that consist of contact area and void area. Theoretically, non-welded contacts are represented by discontinuous boundary conditions [11, 24]. Two non-effervescent waves are found to exist: a fast (symmetric) wave and a slow (anti-symmetric) wave. These waves are dispersive and their existence depends on the frequency of the signal and the specific stiffness of the fracture. Interface waves only exist when the shear polarization of the wave is perpendicular to the fracture. For single fractures, the group velocity ranges between the Rayleigh velocity and the bulk-shear velocity for a welded surface [6].

In this paper we will show that interface waves exist along the intersection between two orthogonal fractures and that the velocity of these "intersection waves" depends on the stress condition along the intersection. We have also observed that for very low stresses intersection waves travel with group velocities below the Rayleigh wave velocity.

2. Experiment. To investigate seismic waves propagating along single and orthogonal fractures, two aluminum samples were used. Fig. 1 shows the aluminum samples used in the experiment, one solid and one quartered. Both samples measured 150 mm x 150 mm x 100 mm and were machined smooth, i.e. no visible roughness. Aluminum was chosen to eliminate any effects from the background matrix or anisotropy within the material. The solid aluminum sample was used as a control for comparison to the quartered aluminum sample (Fig. 1 right).

Arrays containing nine transducers (Olympus - Panametrics V153 and V103 with a central frequency ~ 1 MHz) were used to propagate and receive shear (S) and compressional (P) seismic waves that were propagated through the samples. The transducers were coupled using honey that

---

*Department of Physics, Purdue University, West Lafayette, IN, USA
†School of Civil Engineering, Purdue University, West Lafayette, IN, USA
‡Department of Physics, Department of Earth and Atmospheric Science, and School of Civil Engineering, Purdue University, West Lafayette, IN, USA
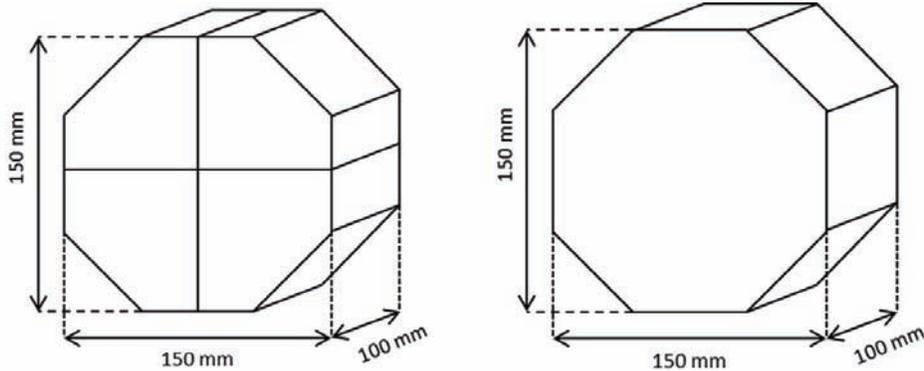
FIGURE 1. *Aluminum samples: (left) quartered sample with intersecting orthogonal fractures, and (right) solid sample.*
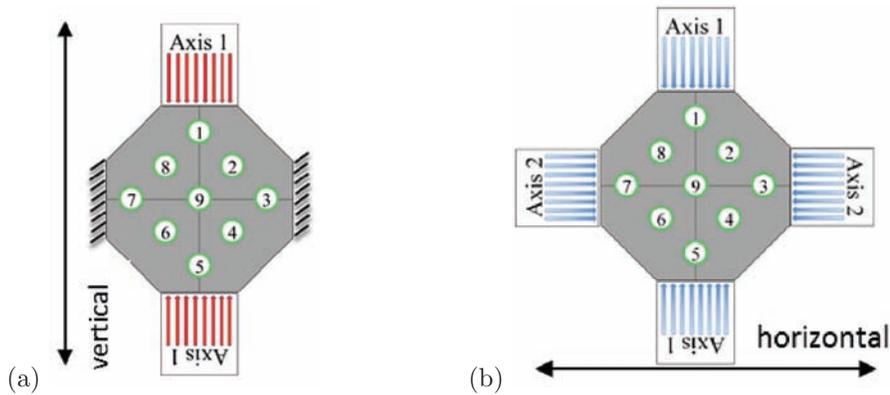

FIGURE 2. *A sketch of the loading configurations is shown for (a) Single axis loading with confinement in the horizontal direction and for (b) bi-axial loading of a sample. The green circles represent the transducer location and numbering. Vertical and horizontal are marked for reference to transducer polarization. The drawing is not to scale.*

was baked to remove 8.75% of water by mass. A platen was used to hold the transducers against the 150mm x 150mm face of the samples.

A square wave pulse generator (Olympus 5077PR) was used to excite the source transducers using 400V with a repetition rate of 100 Hz. A National Instruments PXI-1042 controller with a PXI-5122 digitizer recorded the transmitted signals and stored them for analysis.

The samples were loaded in a bi-axial loading frame by applying a vertical (Axis 1) load from a SATEC systems model 120CS-1015 loading frame and a horizontal (Axis 2) load from a Flatjack Enerpac RSM50 A4604C hydraulic pump. The axes and directions of loading are shown in Fig. 2.

Three loading conditions were investigated in this experiment. Loading case A (Fig. 2a) applied $0 - 66.7$kN to axis 1 starting with 5 increments of 4.4kN followed by two 22.2 kN increments; while axis 2 was confined so that it could not expand, but had no applied external load. For case B, axis 1 was confined while axis 2 was loaded from $0 - 66.7$kN for the same loading steps as above. Finally, in case C (Fig. 2b) axis 1 is loaded first to 22.2kN and held at a constant load while axis 2 was

For brevity the polarization of the transducers will be referred to as SH (shear-horizontal) and SV (shear-vertical) where horizontal and vertical are shown in Fig. 2.

3. Results.

3.1. Solid Aluminum. Source-receiver pairs 2, 4, 6, and 8 were used to monitor the intact portions (i.e., no fractures) of the sample during the different loading conditions. Fig. 3 shows the
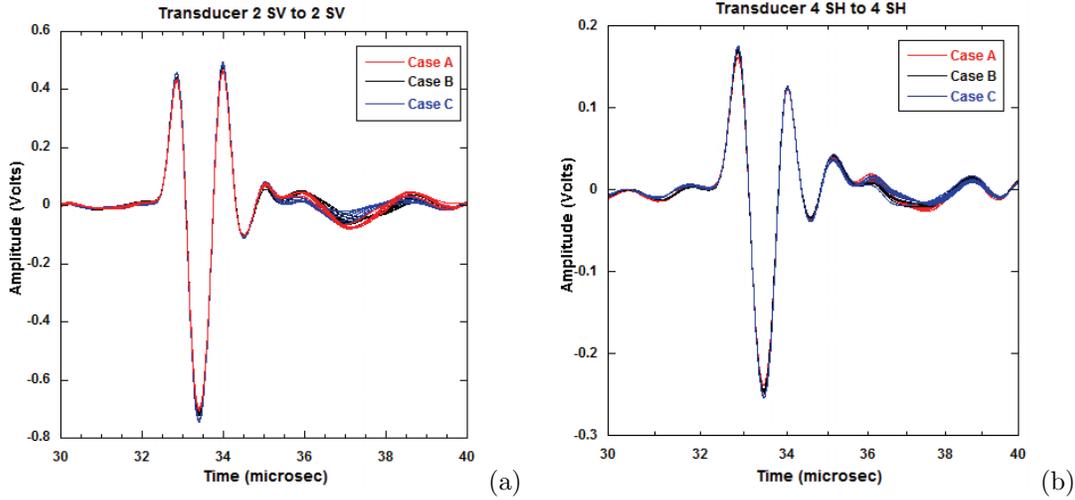
FIGURE 3. *a) Waveform of transducer 2 SV showing bulk-shear waves for all three loading cases. b) Waveform of transducer 4SH showing the same bulk-shear wave traveling through solid aluminum. The variation in the waves for times > 36 microseconds is due to honey coupling.*

received shear signals for cases A, B and C recorded for a vertical shear wave polarization (2SV) and a horizontal shear wave polarization (4SH). The shear waves propagated through the intact portions of the sample were insensitive to changes in stress. However, the aluminum did exhibit slight shear wave anisotropy.

The velocities in the horizontal direction, i.e. V2SH = 3037 m/s, was found to be less than in the vertical direction, i.e. V4SV= 3059 m/s. This was observed for all transducers locations. The aluminum had little effect on the waveforms because the intact portion of the sample does not contain micro-cracks. The small variations observed in the later part of the signal (> 36 microseconds) are from honey coupling variations, and were observed in the data from all samples and from all transducers.

3.2. Single Fractures. Transducer pairs 1, 3, 5 and 7 were used to study the behavior of a single fracture under the three loading conditions in the quartered sample (Fig. 1 left). The vertical fracture was interrogated using pairs 1 and 5, while pairs 3 and 7 probed the horizontal fracture. When any of the shear transducers were polarized parallel to the fracture, i.e. 1SV or 3SH, the same bulk –shear wave observed in the solid aluminum was found (Fig. 4a). When the transducer was polarized perpendicularly to the fracture, i.e. 1SH or 3SV, interface waves were observed that exhibited stress-dependence for all loading cases (Fig. 4b).

The stress-dependent interface waves shown in Fig. 4b arrived earlier for higher applied stress than lower stresses, and also had a decrease in amplitude for increasing applied load. The same trend was observed for all interface waves measured with transducers polarized perpendicularly to a single fracture. This trend indicates that as the fracture was closing, with increasing load, the seismic waves were becoming more like the bulk shear waves of Fig. 4a because the contact area in the fracture increases with increasing load.

3.3. Orthogonal Fracture Intersection. Transducer pair 9 (Fig. 2) were the only transducer that sampled the orthogonal fracture intersection. Measurements were made in the intersection for both shear-wave polarizations because the transducer was always perpendicular to one of the fractures (Fig. 5).

Unlike the single fracture interface waves these waveforms were found to exhibit different behavior for each polarization for the same loading conditions. From transducer pair 9 SV measurements, the velocity of the wave along the intersection increased with increasing applied load for loading
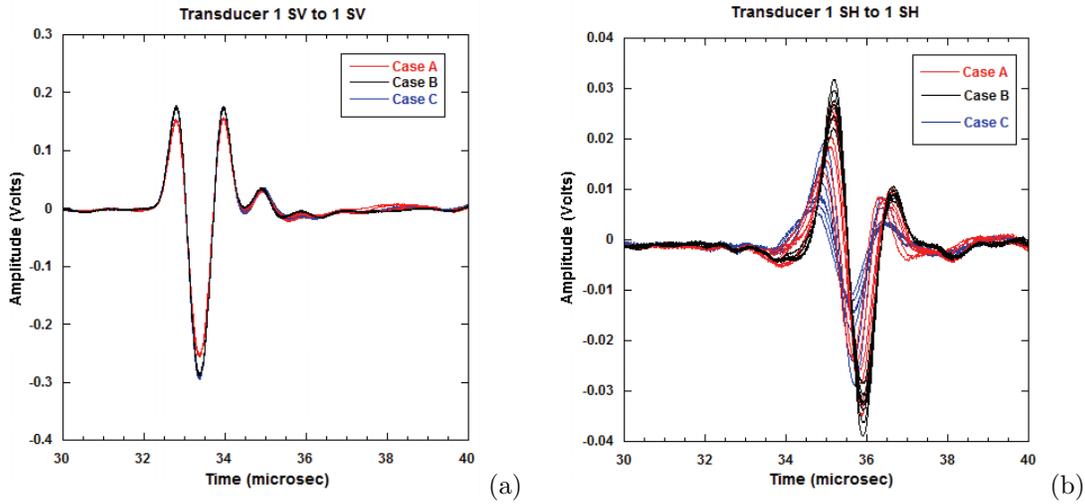
FIGURE 4. *Waveforms showing (a) the bulk-shear wave measured by transducer pair 1SV polarized parallel to the vertical fracture; and (b) interface waves measured by transducer pair 1SH polarized perpendicularly to the horizontal fracture. The different lines of the same color represent different loading values.*
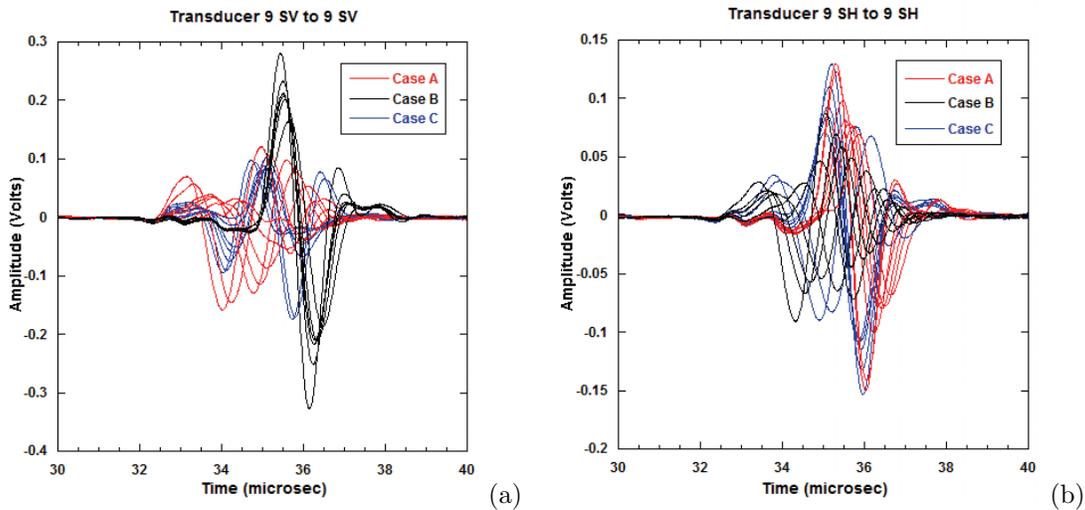

FIGURE 5. *Waveforms showing large stress dependence from a) transducer pair 9 SV for all loading cases and b) transducer pair 9 SH for all loading cases. The different lines of the same color represent different loading conditions.*

cases A and B, but decreased in velocity for case C (Fig. 5a). However, the amplitude of the intersection wave increased for loading cases A and B, but not for case C. The intersection waves measured with transducer pair 9 SH (Fig. 5b), exhibited an increase in velocity for all three loading cases with an increase in amplitude for case A and B, but a decrease in amplitude for case C.

4. Analysis. A Morlet-wavelet technique was used to analyze the time-frequency behavior of the signals and to calculate the group velocity [25]. This method was applied to the data from the transducers polarized perpendicularly to the single fractures, both polarizations on the fracture intersection and from the intact portions of the sample.

4.1. Single Fracture Analysis. Using the wavelets obtained from the signals of transducer pairs 1 and 7, the group velocity was measured for the maximum amplitude in the wavelet at 0.70 ± 0.01 MHz. This frequency was the dominant frequency for nearly all transducers in the intact
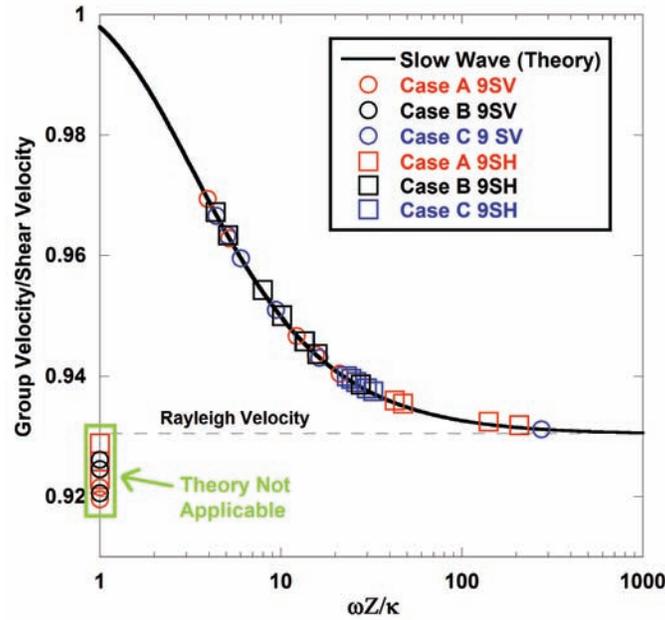
FIGURE 6. *Normalized Group velocity as a function of normalized fracture specific stiffness. All three cases for transducer 9 SV and 9 SH are fit to the slow wave. Those values on the y-axis, below the Rayleigh velocity were found to be lower than the Rayleigh velocity and thus could not be used to estimate a specific stiffness. Error bars are approximately the size of the symbols.*

and fractured samples. This was done at each loading condition in all three cases.

Interface wave theory [24] was used to estimate the fracture specific stiffness of the single fractures using the measured group velocities, the frequency and the impedance of the sample. Because only shear wave transducers were used, it was assumed that only the slow interface waves were observed in these experiments.

By fitting the measured frequency (0.70 MHz) and velocity, an estimate for the specific stiffness was obtained. All measured velocities for interface waves from a single fracture fell within the expected range, i.e. between the Rayleigh velocity and the bulk shear wave velocity, and were found to agree with previous experiments on single fractures [6, 7, 11, 12].

4.2. Fracture Intersection Analysis. The same analysis was performed on the data from the fracture intersection for both shear-wave polarizations. The measured group velocities were then compared to the expected velocities from the fracture interface wave theory. For case A and B at low applied loads (<13 kN) the measured velocities were below the Rayleigh velocity (circled region in Fig. 6). Above 13kN the velocity was found to fall back within the expected range of velocities for an interface wave. For case C all measured velocities were within the expected range.

Fig. 6 shows the measured group velocities for transducer 9 fit to normalized velocity as a function of normalized specific stiffness ($\omega Z/\kappa$). The labels below the Rayleigh velocity line were those values that had measured velocities lower than the Rayleigh velocity.

This is the first experimental result that has measured waves along a fracture slower than the Rayleigh-wave velocity. Intersection waves may be a distinct coupled-guided-mode and not just an interference of interface waves. Additional research is needed to develop a theoretical understanding of this potentially new wave.

5. Computational Modeling.

5.1. Numerical Simulation. To develop a better understanding of the stiffness and stress distribution along the fracture intersection, a numerical simulation to estimate the stress distribution

TABLE 4.1
Values from transducer 9 used in calculating the theoretical curves of Fig. 6. Velocities were measured using the solid aluminum sample (Fig. 1, right).

Compressional Velocity	5927 m/s
Shear Velocity SV	3056 m/s
SH	3037 m/s
Density	2700 kg/m^3
Material	Aluminum
Frequency	0.70 MHz

within the sample and along the fracture plane was performed using a commercial finite element program ABAQUS.

The quartered aluminum sample (Fig. 1, left) was assumed to behave elastically and Coulomb friction was used to model the frictional characteristic of the fracture planes. Coulomb friction assumes that shear resistance of a fracture is linearly proportional to the product of the friction coefficient and normal stress such that there is no slip if mobilized shear stress is less than the shear resistance. The frictional coefficient of tan 10° was used in the simulation. The applied load in the experiment was numerically simulated by uniformly distributed pressure and the displacement at the horizontal centerline of the sample was constrained by installing rollers on the horizontal fracture to reflect the symmetricity of the sample.

Fig. 7 shows the horizontal and vertical stress distributions by numerical simulation in the sample corresponding to the loading case C. Recall that for case C the vertical load was applied to the sample first $(0 - 22.2$ kN$)$, and then the horizontal load was applied $(0 - 67$ kN$)$. The same loading condition was simulated in ABAQUS.

The stress distribution in Fig. 7 shows how the stress acting on the fracture intersection changes with increasing applied load. For horizontal stress, the intersection experiences an increase in compression when the load on axis 2 increases from 22.2 kN to 66.7 kN (Fig. 7 left). Since the load on axis 2 is also horizontal, this makes sense that the stress would increase. The vertical stress at the intersection is in compression at low applied loads (Fig. 7 right top) but in tension as the load on axis 2 increases, indicating that the fracture intersection is closed horizontally but opened vertically.

5.2. Comparison to Experiment. The numerical results were analyzed at the same location as the transducers used to measure the single fracture and intersection interface waves in Fig. 2. Although stress was not directly measured in the experiment, the fitted stiffnesses are related to the stress by the geometry of the fractures. As normal stress is applied to a fracture, the apertures reduce and the contact area increases, i.e. the fracture specific stiffness increases. Fig. 8 compares the variation of (a) experimentally estimated fracture stiffness with (b) stress normal to the fracture plane as a function of applied load on axis 2. For 9 SV, the fracture stiffness decreases as the axis 2 load increases, which agrees well with the decrease of normal stress at the location of transducer 9. The overall trends of the variations of fracture stiffness for transducer 7 SV and 1 SH in Fig. 8a are in relatively good agreement with that of the numerically determined normal stress at the corresponding transducer location in Fig. 8b. Only 9 SH showed the difference between the variation of stiffness and the normal stress.

6. Conclusion. Experimental and numerical studies of single and orthogonal intersecting fractures were performed to explore the fracture specific stiffness using seismic waves. A quartered aluminum sample was used to measure the shear waves both through the solid and fractured portions.

Bulk-shear waves were observed to propagate through the solid portions of the aluminum, and as expected were stress-dependent interface waves along the single fractures. Waveform and wavelet analysis of the single fractures resulted in a range of group velocities and fracture specific stiffness values between the Rayleigh velocity and bulk shear velocity, showing agreement with previous
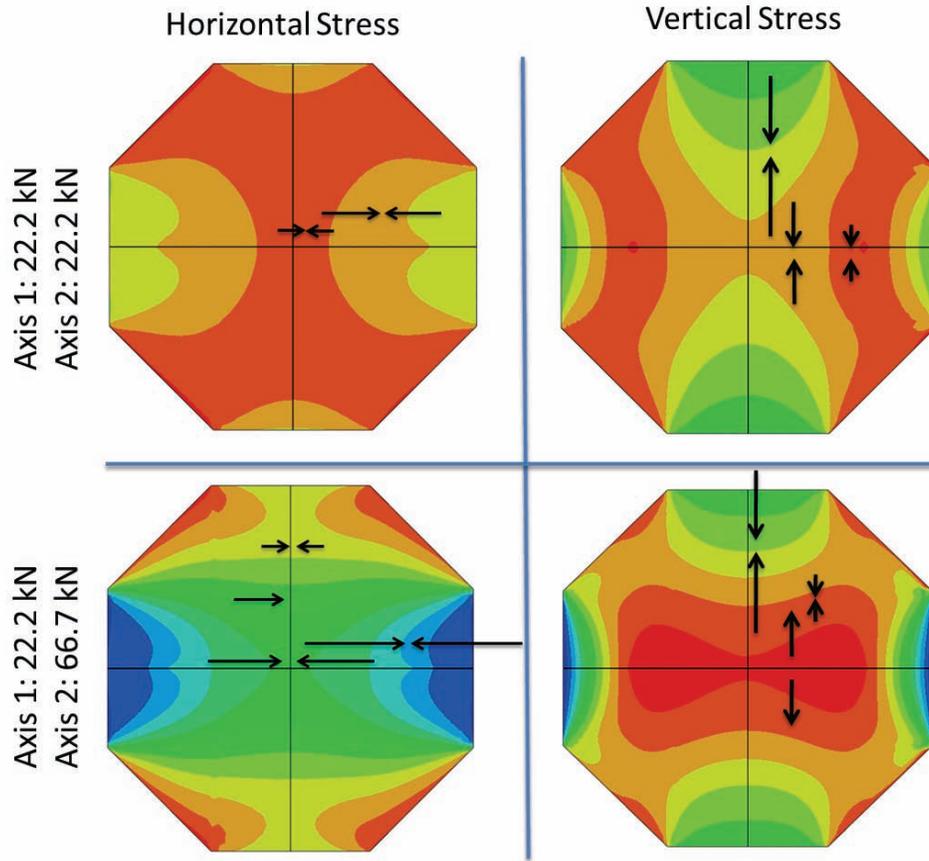
FIGURE 7. *Stress analysis from ABAQUS with arrows indicating the stress direction for the load with arrow length indicating relative magnitude. Case C shown. As the load on axis 2 increases the stress at the fracture intersection compresses horizontally, but expands vertically.*
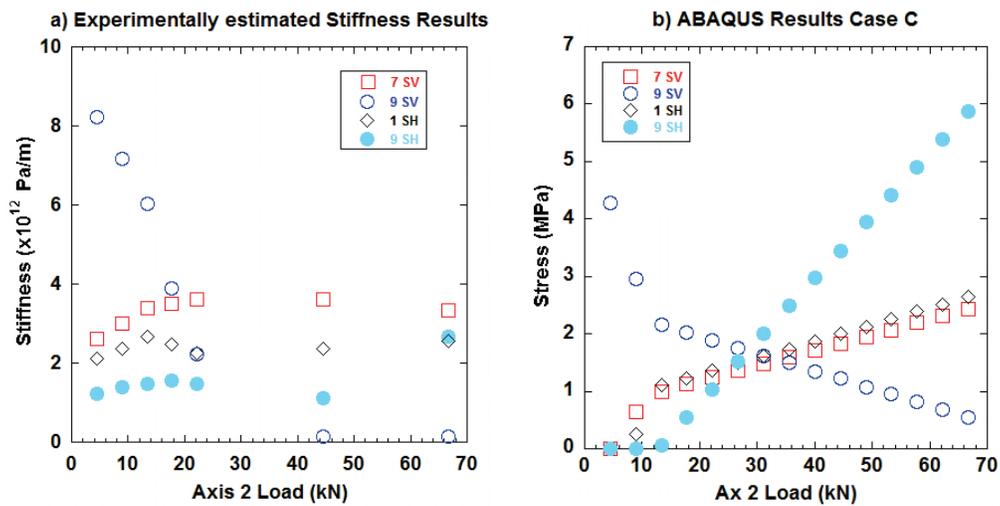

FIGURE 8. *a) Experimentally estimated fracture specific stiffness as a function of Axis 2 loading for case C. Transducers 1, 7, and 9 are shown. b) Numerical results for stress as a function of Axis 2 load for case C. The locations correspond to the same locations as transducer 1, 7, and 9.*

experiments [5-13].

At the orthogonal fracture intersection a stress-dependent wave was also observed, but not a regular interface wave. This new wave was found to have different trends with increasing applied load, and the measured group velocities were not within the expected range. At low applied loads (< 13 kN) the velocity was found to be below the Rayleigh wave velocity for cases A and B. Estimated specific stiffness values were found to be less than, equal to, or below the stiffness values measured on a single fracture.

To understand the observed stiffness of the fracture intersection, a numerical simulation of stress was conducted using ABAQUS. Results for case C demonstrated that when the sample was loaded vertically the vertical fracture intersection opened; after horizontal loading the fracture was found to close causing the non-linearity observed in stress vs. load in Fig. 8.

This study has demonstrated that shear specific stiffness of fracture intersections is not the same as the individual intersecting fractures because stress distributions along a fracture are a function of loading conditions and the number of fractures. Although numerical simulations appear to reproduce the trend in the result, a theoretical understanding of the intersection interface waves must be found.

Future work will involve theoretical analysis of the intersection interface waves to determine if they are some sorts of guided-mode of interface waves, or some other wave entirely.

References.

1. Hast, N., *The existence of Horizontal Stress Fields and Orthogonal Fracture Systems in the Moon's Crust.* Modern Geology, 1973. **4**: p. 73-84.

2. Bai, T., et al., *Orthogonal Cross Joints: do they imply a regional stress rotation?* Structural Geology, 2002. **24**: p. 77-88.

3. Storetvedt, K.M. and A.E. Scheidegger, *Orthogonal joint systems in the Bergen Area, Southwest Norway, and their regional significance.* Physics of the Earth and Planetary Interiors, 1992. **73**: p. 255-263.

4. Gross, M.R., *The origin and spacing of cross joints: examples from the Monterey Formation, Santa Barbara Coastline, California.* Structural Geology, 1993. **15**(6): p. 737-751.

5. Pyrak-Nolte, L.J., L. Myer, and N.G. Cook, *Transmission of Seismic Waves Across Single Natural Fractures.* Geophysical Research, 1990. **95**(B6): p. 8617-8638.

6. Pyrak-Nolte, L.J., J. Xu, and G. Haley, *Elastic Interface Waves Propagating in a Fracture.* Physical Review Letters, 1992. **68**(24): p. 3650-3653.

7. Nihei, K., et al. *Elastic Interface wave propagation along a fracture.* in *International Congress on Rock Mechanics.* 1995. Tokyo, Japan: International Society for Rock Mechanics.

8. Gu, B., et al., *Incidence of plane waves upon a fracture.* Geophysical research, 1996. **101**(B11): p. 25337-25346.

9. Gu, B., et al., *Fracture interface waves.* Geophysical research, 1996. **101**(B1): p. 827-835.

10. Gu, B., K. Nihei, and L. Myer, *Numerical simulation of elastic wave propagation in fractured rock with the boundary integral equation method.* Geophysical Research, 1996. **101**(B7): p. 15933-15943.

11. Pyrak-Nolte, L.J., S. Roy, and B. Mullenbach, *Interface Waves Propagatied Along a Fracture.* Applied Geophysics, 1996. **35**: p. 79-87.

12. Xian, C., D.D. Nolte, and L.J. Pyrak-Nolte, *Compressional Waves Guided Between Parallel Fractures.* Rock Mechanics & Mining Sciences, 2001. **38**: p. 765-776.

13. Nakagawa, S., K. Nihei, and L. Myer, *Elastic Wave Propagation Along a set of Parallel Fractures.* Geophysical Research Letters, 2002. **29**(16).

14. Johnson, J. and S. Brown, *Experimental mixing variability in intersecting natural fractures.* Geophysical Research Letters, 2001. **28**(22): p. 4303-4306.

15. Glass, R.J., et al., *Unsaturated flow through a fracture-matrix network: Dynamic preferential pathways in mesoscale laboratory experiments.* Water Resources Research, 2002. **38**(12, 1281).

16. Wood, T.R., M.J. Nicholl, and R.J. Glass, *Fracture intersections as integrators for unsaturated flow.* Geophysical Research Letters, 2002. **29**(24, 2191).

17. Glass, R.J., et al., *Unsaturated flow through fracture networks: Evolution of liquid phase structure, dynamics, and the critical importance of fracture intersections.* Water Resources Research, 2003. **39**(12, 1352).

18. Park, y.-J., et al., *Transport behavior in three-dimensional fracture intersections.* Water Resources Research, 2003. **39**(8, 1215): p. 1-9.

19. Wood, T.R., M.J. Nicholl, and R.J. Glass, *Influence of fracture intersections under unsaturated, low-flow conditions.* Water Resources Research, 2005. **41**(W04017): p. 1-17.

20. Bagheri, M.A. and A. Settari, *Effects of fractures on reservoir deformation and flow modeling.* Canadian Geotechnical Journal, 2006. **43**: p. 574-586.

21. Johnson, J., S. Brown, and H. Stockman, *Fluid flow and mixing in rough-walled fracture intersections.* Geophysical Research, 2006. **111**(B12206): p. 1-16.

22. Michalis, V.K., et al., *Mixing within fracture intersections during colloidal suspension flow.* Water Resources Research, 2009. **45**(W08429): p. 1-10.

23. Zhang, Y., C.M. Sayers, and J.I. Adachi, *The use of effective medium theories for seismic wave propagation and fluid flow in fractured reservoirs under applied stress.* Geophysical Research, 2009. **177**: p. 205-221.

24. Pyrak-Nolte, L.J. and N.G. Cook, *Elastic Interface Waves Along a Fracture.* Geophysical Research Letters, 1987. **14**(11): p. 1107-1110.

25. Pyrak-Nolte, L.J. and D.D. Nolte, *Wavelet Analysis of velocity dispersion of elastic interface waves propagating along a fracture.* Geophysical Research Letters, 1995. **22**(11): p. 1329-1332.